AJNR

Susceptibility changes on preoperative acetazolamideloaded 7T MR quantitative susceptibility mapping predict post-carotid endarterectomy cerebral hyperperfusion

Kazuto Kimura, Yosuke Akamatsu, Kentaro Fujimoto, Ikuko Uwano, Makoto Sasaki, Shunrou Fujiwara, Masakazu Kobayashi, Takahiro Koji, Kenji Yoshida, Kazunori Terasaki and Kuniaki Ogasawara

AJNR Am J Neuroradiol published online 5 February 2025
http://www.ajnr.org/content/early/2025/02/05/ajnr.A8692

ORIGINAL RESEARCH

Susceptibility changes on preoperative acetazolamide-loaded 7T MR quantitative susceptibility mapping predict post-carotid endarterectomy cerebral hyperperfusion

Kazuto Kimura, Yosuke Akamatsu, Kentaro Fujimoto, Ikuko Uwano, Makoto Sasaki, Shunrou Fujiwara, Masakazu Kobayashi, Takahiro Koji, Kenji Yoshida, Kazunori Terasaki, and Kuniaki Ogasawara

ABSTRACT

BACKGROUND AND PURPOSE: Post-carotid endarterectomy (CEA) cerebral hyperperfusion (CH) can cause intracerebral hemorrhage and cognitive decline. Alterations in susceptibility in response to acetazolamide (ACZ) on 7T MRI quantitative susceptibility mapping (QSM) detects elevated CBV occurring due to impaired cerebrovascular autoregulation. We explored preoperative relative susceptibility changes on 7T MRI QSM in response to ACZ and their ability to predict CH following CEA.

MATERIALS AND METHODS: Sixty-three patients with uni- or bilateral cervical ICA stenosis ≥70% underwent 7T MRI at baseline and at 5, 10, 15, and 20 min after ACZ administration before surgery. The difference between the susceptibility of venous structures and surrounding brain parenchyma at each time point after ACZ administration relative to the difference at baseline (relative susceptibility difference; RSD) on QSM images was calculated in the cerebral hemisphere ipsilateral to surgery. Brain perfusion SPECT was conducted preoperatively and immediately following CEA to detect postoperative CH (≥ 100% rise in CBF postoperatively).

RESULTS: In nine patients with postoperative CH, RSD was significantly increased at 5 or 10 min following ACZ administration ($p < 0.05$) but reduced at 15 and 20 min ($p < 0.05$). In 54 patients without postoperative CH, RSD at all four time points after ACZ administration was significantly lower than the baseline value ($p < 0.05$). The area under the receiver operating characteristic curve to predict postoperative CH was significantly greater in RSD_5 (0.981; 95% CI, 0.910–0.999) than in RSD_{15} (0.872; 95% CI, 0.764–0.943) ($p < 0.05$) or RSD_{20} (0.780; 95% CI, 0.658–0.874) ($p < 0.01$). Sensitivity, specificity, and positive and negative predictive values for RSD_5 at a cutoff near the left upper corner of the curve were 100%, 89%, 60%, and 100%, respectively. Logistic regression analysis revealed that only RSD_5 significantly predicted postoperative CH (95% CI, 455.9–4043.6; $p < 0.05$).

CONCLUSIONS: Changes in susceptibility on preoperative 7T MRI QSM following ACZ administration predict CH following CEA. Patients with increased RSD_5 on pre-CEA 7T MRI QSM following ACZ administration should undergo brain perfusion imaging immediately after surgery. Detection of CH on postoperative brain perfusion imaging warrants intensive blood pressure control.

ABBREVIATIONS: CEA = carotid endarterectomy; CH = cerebral hyperperfusion; OEF = oxygen extraction fraction; ACZ = acetazolamide; QSM = quantitative susceptibility mapping; 3D = three-dimensional; RSD = relative susceptibility difference; SD = standard deviation; ROC = receiver operating characteristic.

Received October 4, 2024; accepted after revision February 1, 2015.
From the Department of Neurosurgery (K.K., Y.A, K.F., M.K, T.K., K.Y., K.O.), the Centre for Division of Ultrahigh Field MRI, Institute for Biomedical Sciences (I.U., M.S), the Division of Molecular and Cellular Pharmacology, Department of Pathophysiology (S.F.), and the Cyclotron Research Center (K.T.), Iwate Medical University, Yahaba, Japan.

Kuniaki Ogasawara has a conflict of interest as follows: Consigned research fund from Nihon Medi-Physics Co., Ltd.

Correspondence to Kuniaki Ogasawara, M.D., Department of Neurosurgery, Iwate Medical University, 1-1-1 Idaidoori, Yahaba-cho, Iwate 028-3694, Japan, E-mail: kuogasa@iwate-med.ac.jp

SUMMARY SECTION

PREVIOUS LITERATURE: Whereas static images of susceptibility differences between venous structures and surrounding brain tissue generated from quantitative susceptibility mapping (QSM) without acetazolamide (ACZ) challenge reportedly reflect post-carotid endarterectomy (CEA) cerebral hyperperfusion (CH) risk, these images cannot detect stage I hemodynamic impairment, resulting in false negatives and a relatively low positive predictive value for predicting CH after CEA.

KEY FINDINGS: Changes in susceptibility differences on preoperative 7T MRI QSM following ACZ administration accurately predict CH following CEA.

KNOWLEDGE ADVANCEMENT: Patients with increased susceptibility differences at 5 min after ACZ administration on pre-CEA 7T MRI QSM should undergo brain perfusion imaging immediately after surgery. CH detected on postoperative brain perfusion imaging warrants intensive blood pressure control.

Copyright 2025 by American Society of Neuroradiology.

INTRODUCTION

Post-carotid endarterectomy (CEA) cerebral hyperperfusion (CH) involves substantial elevation in ipsilateral CBF that exceeds the metabolic needs of brain.[1,2] CH syndrome is defined by the development of symptoms due to CH, including unilateral headache, seizures, and neurological deficits secondary to intracerebral hemorrhage.[1-5] CH syndrome almost always occurs among patients with CBF increases exceeding 100% following CEA.[6] Notably, CH syndrome can cause irreversible cognitive decline even in the absence of hemorrhage, likely due to damage to the blood brain barrier and leakage of toxic substances causing diffuse damage to the ipsilateral cerebral cortex and white matter.[7-10] This has been reported even in asymptomatic patients with post-CEA CH, and is thought to be a significant contributor to postoperative cognitive decline after CEA.[7-9]

When cerebral perfusion pressure decreases due to the chronic progression of carotid stenosis, cerebrovascular autoregulatory mechanisms attempt to maintain CBF by dilating precapillary resistance vessels (stage 1 ischemia), resulting in CBV increase (Online Supplemental Data).[11–13] As cerebral perfusion pressure declines further, continuous maximal dilation of precapillary resistance vessels eventually exhausts cerebrovascular autoregulatory mechanisms and CBF starts to decline (stage 2 ischemia or misery perfusion) (Online Supplemental Data).[11–13] Oxygen extraction fraction (OEF) increases in stage 2 ischemia to maintain oxygen metabolism.[11–13] Patients with decreased cerebrovascular reactivity in the hemisphere ipsilateral to CEA are at risk of CH after surgery.[4, 14-16]

Although several studies have demonstrated preoperatively elevated CBV, assessed using perfusion-weighted imaging or intravoxel incoherent motion MRI as an independent predictor of post-CEA CH,[18,19] positive predictive values for these CBV qualitative measurements in predicting post-CEA CH were < 50%.[18,19] Methods that can identify exhausted cerebrovascular autoregulation with higher specificity, by assessing not only increased CBV but also increased OEF, are therefore needed to achieve more accurate prediction of post-CEA CH. Another limitation of qualitative CBV assessment using perfusion-weighted imaging or intravoxel incoherent motion MRI is that these methods rely on affected-to-contralateral asymmetry to identify high CBV and are therefore limited to use in patients with unilateral disease.[18,19]

Cerebrovascular reserve can be measured, and hemodynamic impairment identified and staged, using a vasodilatory stimulus such as acetazolamide (ACZ) challenge.[21] Decreased cerebrovascular reactivity on the ACZ challenge reportedly offers a significant predictor of post-CEA CH.[14-16] A study investigating chronological changes in CBF following ACZ administration using ^{15}O-gas PET found that while CBF continued to rise up to 15 min following ACZ administration in regions with normal hemodynamics, it transiently decreased at 5 min post-administration before rising again at 15 min in regions with elevated CBV compared to pre-administration levels.[22] This paradoxical, transient reduction in CBF immediately after ACZ administration is known as the early “steal” phenomenon and indicates exhausted cerebrovascular reactivity precluding a vasodilatory response.[22] Blood flow is “stolen” away by vascular territories with intact cerebrovascular reactivity which mount a vasodilatory responses to increase CBF.

MRI can quantify blood-oxygen-level-dependent changes in venous structures and brain parenchyma, induced by differences in magnetic susceptibility between oxyhemoglobin and deoxyhemoglobin.[23–25] Quantitative susceptibility mapping (QSM) is a novel post-processing technique that yields quantitative measurement of magnetic susceptibility from a single MRI phase image acquisition.[23] QSM using a 7T scanner offers profound susceptibility effects and optimized post-processing techniques.[26] As a result, QSM enables assessment of OEF.[26] The scan time for QSM is also relatively brief (3 min and 25 s), allowing dynamic imaging of blood oxygenation alterations in venous structures and brain parenchyma.[27] OEF in areas with the "steal" phenomenon in CBF shows transient increases as CBF decreases. The "steal" phenomenon in CBF can thus, at least theoretically, be detected as an increase in susceptibility on QSM, provided cerebral metabolism remains unchanged by ACZ. In fact, susceptibility reportedly increased at 5 or 10 min post-ACZ administration in the cerebral hemisphere with elevated CBV compared to pre-administration levels.[27]

Considering this background, we explored whether dynamic changes in susceptibility after ACZ administration, as measured by 7T MRI QSM before surgery, can predict post-CEA CH.

MATERIALS AND METHODS

All study procedures involving human participants were conducted in accordance with the guidelines of the institutional ethics committee. Written informed consent was obtained from participants or their next of kin. The methodology proposed in the STARD checklist was followed.

Inclusion criteria

Consecutive individuals who met the following inclusion criteria were prospectively selected: (1) uni- or bilateral cervical ICA stenosis ≥ 70%, as defined by the North American Symptomatic Carotid Endarterectomy Trial criteria, confirmed via catheter-based angiography;[28] (2) preoperative modified Rankin Scale score of 0–2; and (3) asymptomatic status, defined as the absence of ipsilateral carotid territory ischemic symptoms for more than 6 months prior to presentation, or symptomatic status, defined as the presence of ipsilateral carotid territory ischemic symptoms between 2 weeks and 6 months before presentation. Individuals who were not subjected to preoperative ACZ-loaded 7T MRI or CEA were excluded.

MRI protocol and generation of QSM

ACZ-loaded MRI QSM studies were conducted using a 7T MRI scanner (Discovery MR950; GE Healthcare, Milwaukee, WI) with quadrature transmission and 32-channel receive head coils within 7 days prior to surgery. QSM source data were acquired using a three-dimensional (3D) spoiled gradient-recalled acquisition sequence with flow compensation (TR, 30 ms; TE, 15 ms; flip angle, 20°; FOV,

256×192 mm; acquisition matrix size, 512 × 256; slice thickness, 2 mm; number of slices, 40; number of excitations, 1; receiver bandwidth, 62.5 kHz; and scan time, 3 min 25 s).[26,27] The imaging slab covered from the level of the superior cerebellar peduncle to the high convexity at 80 mm (2 mm×40 slices), and sections were set in the orthogonal axial plane.[26,27] Parallel imaging was not used. After zero-fill interpolation, the dimensions of the final volume size were 512×512×160.[26,27] Magnitude and real/imaginary phase images were obtained from this acquisition with the same volume.[26,27]

ACZ-loaded MRI QSM studies were performed according to a previously described protocol.[27] Briefly, each patient first underwent the MR scanning at baseline. Subsequently, ACZ (1,000 mg, range 13–19 mg/kg body weight) dissolved in 20 mL of physiological saline was injected intravenously over 1 min. MRI scans were then performed four additional times, with mid-scan times set at 5, 10, 15, and 20 min following the completion of ACZ administration.

As outlined in earlier methods (Online Supplemental Data),[26,27] images of susceptibility differences between the average susceptibility of small veins and surrounding tissue were generated from QSM images using a method similar to that described in the previous study.[26,27]

Brain perfusion SPECT (Online Supplemental Data)

Image data analyses

Images were analyzed according to previously described methods.[26,27] All QSM-generated susceptibility difference and brain perfusion SPECT images were transformed to the standard brain size and shape using both linear and nonlinear transformations with Statistical Parametric Mapping version 12 (SPM12; Wellcome Department of Imaging Neuroscience, University College London, UK).[29] A total of 318 constant ROIs were automatically placed in both the cerebral and cerebellar hemispheres using a 3D stereotaxic ROI template in SPM.[30] These ROIs were grouped into 10 segments per hemisphere—callosomarginal, pericallosal, precentral, central, parietal, angular, temporal, posterior, hippocampal, and cerebellar—based on arterial supply. Five of the 10 segments (precentral, central, parietal, angular, and temporal), perfused by the MCA, were defined as the MCA ROI (Online Supplemental Data).[27]

The difference in average susceptibility between small venous structures and surrounding brain tissue on QSM-generated susceptibility difference images was measured in the MCA ROI of the cerebral hemisphere ipsilateral to surgery using image analysis software (ITK-SNAP; www.itksnap.org).[31] In the MCA ROI, relative susceptibility difference (RSD, %) was calculated as 100 × susceptibility difference at each time (5, 10, 15, or 20 min) after ACZ administration on QSM images/susceptibility difference at baseline on QSM images.

For the brain perfusion SPECT images, the mean quantitative CBF of all pixels in the MCA ROI of the cerebral hemisphere ipsilateral to surgery was determined pre- and postoperatively. Post-CEA CH was defined as a quantitative CBF increase of ≥100% compared to the preoperative value.[3,16]

Pre-, intra-, and postoperative management (Online Supplemental Data)

Statistical analysis (Online Supplemental Data)

The sample size was determined based on prior studies.[18,19] Data are expressed as mean ± standard deviation (SD). When data were not normally distributed, differences were evaluated using the Friedman test, followed by the Conover test as a post-hoc analysis. Receiver operating characteristic (ROC) curves were employed to compare the accuracy of predicting the development of postoperative CH based on RSD at each time point after ACZ administration. Pairwise comparisons of the area under the ROC curve for RSD at each time point were performed. Univariate analysis, employing the Mann–Whitney U test or Fisher's exact test, was performed to explore the relationship between postoperative CH and each variable, including the RSD with the highest area under the ROC curve. Logistic regression analysis of variables associated with CH was performed using a sequential backward elimination approach. Exclusion of explanatory variables was halted when the p-value of the remaining variables reached < 0.2. P-values < 0.05 were considered significant.

RESULTS

During the 36-month study period, 81 patients fulfilled the inclusion criteria and were scheduled to undergo preoperative ACZ-loaded MRI studies. However, 12 patients could not undergo 7T MRI due to the presence of implantable electronic devices or metal implants. In another 3 patients, the 7T MRI was canceled through the scanning process due to the onset of vertigo, phosphenes, or sensations of thermal heat. Consequently, 66 patients successfully completed the 7T MRI. However, 3 patients were excluded from the analysis because sufficient data to generate QSM were not obtained due to motion artifacts. Therefore, 63 individuals were included in the final analysis.

The ages of the 63 patients (58 men and 5 women) was 56–79 years (mean age: 70 ± 6 years). Regarding comorbidities, 53 patients had hypertension, 17 had diabetes mellitus, and 17 had dyslipidemia. In terms of the ICA ipsilateral to surgery, 49 patients had symptomatic lesions, while 14 had asymptomatic lesions. Additionally, 7 patients had an asymptomatic carotid steno-occlusive lesion contralateral to surgery (bilateral steno-occlusive lesions). The degree of ICA stenosis ipsilateral to surgery ranged from 70% to 99% (mean: 88 ± 9%), and the duration of ICA clamping was 13–49 min (mean: 34 ± 8 min). An intraluminal shunt was placed in three patients.

Among the nine patients (17%) who met the CBF criteria for CH on brain perfusion SPECT immediately postoperatively, eight showed resolution of CH by the third postoperative day, and their subsequent courses were uneventful. However, in the remaining patient with persistent CH on the third postoperative day, preexisting hemiparesis on the side contralateral to the surgery worsened 5 days after CEA. This patient was diagnosed with CH syndrome, prompting the induction of a propofol coma. Fortunately, no intracranial hemorrhage developed, and the patient's neurological symptoms eventually resolved. Postoperative courses in the other 54 patients without post-CEA CH were also uneventful. Absence or presence and severity of neurologic deficits thus did not change between before and 1 month after CEA.

All RSD data obtained for each time point in patients with or without postoperative CH showed non-normal distributions. **Figure 1**

illustrates the chronological changes in RSD after ACZ administration in patients with and without CH immediately following surgery. In patients experiencing CH, RSD significantly increased at 5 and 10 min after ACZ administration compared to baseline values, followed by a decrease at 15 and 20 min after ACZ when compared to the values at 5 and 10 min. In contrast, in patients without CH, RSD at all four time points after ACZ administration was significantly lower than the baseline value.

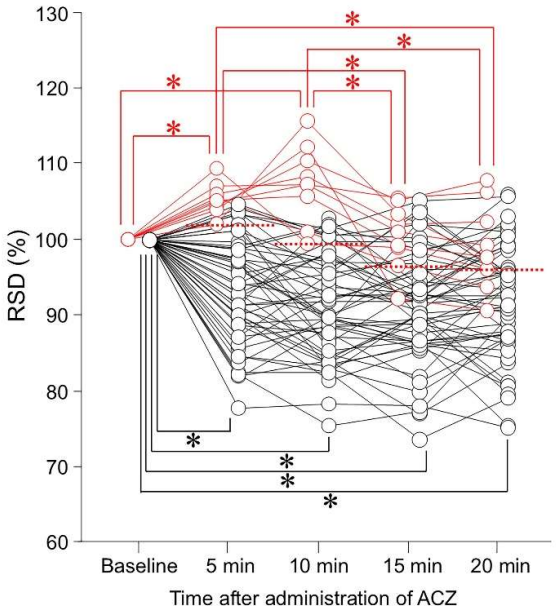

FIG 1. Comparisons of chronological changes in relative susceptibility difference (RSD) after acetazolamide (ACZ) administration between patients with (red circles or solid lines) and without (black circles or solid lines) cerebral hyperperfusion immediately after surgery. Each red dotted horizontal line denotes the cutoff lying closest to the left upper corner of the receiver operating characteristic curve of RSD at each time after ACZ administration for predicting cerebral hyperperfusion. *p < 0.05.

Figure 2 illustrates the comparison of ROC curves for predicting CH immediately after surgery based on RSD at various time points following ACZ administration (Online Supplemental Data). The area under the ROC curve was significantly greater for RSD at 5 min (RSD_5) (0.981; 95% CI, 0.910–0.999) compared to RSD at 15 min (RSD_{15}) (0.872; 95% CI, 0.764–0.943) ($p < 0.05$) and RSD at 20 min (RSD_{20}) (0.780; 95% CI, 0.658–0.874) ($p < 0.01$). Additionally, RSD at 10 min (RSD_{10}) (0.975; 95% CI, 0.901–0.998) demonstrated a significantly greater area than RSD_{20} ($p < 0.05$).

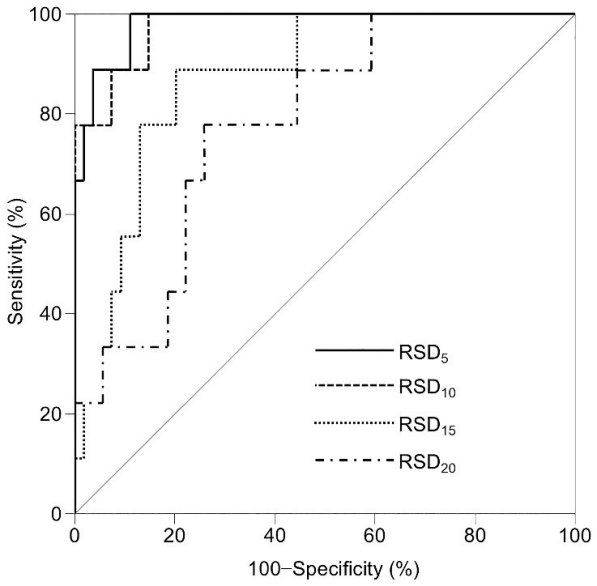

FIG 2. Comparisons of receiver operating characteristic (ROC) curves to predict cerebral hyperperfusion immediately after surgery among RSD at each time point (RSD_5, 5 min; RSD_{10}, 10 min; RSD_{15}, 15 min; RSD_{20}, 20 min) after acetazolamide administration. Area under the ROC curve is 0.981 (95%CI 0.910–0.999) for RSD_5, 0.975 (95%CI 0.901–0.998) for RSD_{10}, 0.872 (95%CI 0.764–0.943) for RSD_{15}, and 0.780 (95%CI 0.658–0.874) for RSD_{20}.

Sensitivity, specificity, and positive and negative predictive values for RSD at each time point after ACZ administration, calculated at a cutoff closest to the upper left corner of the ROC curve for predicting CH, are presented in **Table 1** (Online Supplemental Data). Among these four metrics, RSD_5 exhibited the highest values, followed by RSD_{10}, RSD_{15}, and RSD_{20}, with the exception of sensitivity and negative predictive values, which were both 100% for RSD_5 and RSD_{10}.

Table 1: Sensitivity, specificity, and positive and negative predictive values of preoperative RSD for the prediction of cerebral hyperperfusion following CEA.

Column A	RSD_5	RSD_{10}	RSD_{15}	RSD_{20}
Sensitivity	100%	100%	89%	78%
95% CI	100-100%	100-100%	68-100%	51-100%
Specificity	89%	85%	80%	74%
95% CI	81-97%	76-95%	69-90%	62-86%
Positive-predictive value	60%	53%	42%	33%
95% CI	35-85%	29-77%	20-64%	13-53%
Negative-predictive value	100%	100%	98%	95%
95% CI	100-100%	100-100%	93-100%	89-100%
Cutoff value (%)	102	99	97	96

Table 2 summarizes the risk factors associated with CH development immediately postoperatively. The incidence of bilateral steno-occlusive lesions, the degree of ICA stenosis ipsilateral to surgery, and RSD_5 were significantly higher in individuals with CH immediately after surgery compared to those without CH. Logistic regression analysis in both models with and without multicollinearity (Online Supplemental Data) revealed that only RSD_5 predicted CH immediately after surgery (95% CI, 455.9–4043.6; $p < 0.05$).

Table 2: Risk factors for the development of cerebral hyperperfusion following CEA.

Risk factor	Post-CEA hyperperfusion		p value
	Yes (n = 9)	No (n = 54)	
Age (years) (mean ± SD)	70.0 ± 6.0	70.0 ± 6.1	0.87
Male sex	7 (78%)	51 (94%)	0.15
Hypertension	7 (78%)	46 (85%)	0.63
Diabetes mellitus	2 (22%)	15 (28%)	>0.99
Dyslipidemia	2 (22%)	15 (28%)	>0.99
Symptomatic lesion	8 (89%)	41 (76%)	0.67
Bilateral steno-occlusive lesions	4 (44%)	3 (6%)	<0.01
Degree of ICA stenosis (%) (mean ± SD)	95.0 ± 0.0	87.0 ± 9.6	<0.01
RSD_5 (%) (mean ± SD)	105.4 ± 2.1	93.2 ± 6.7	<0.01
Duration of ICA clamping (min) (mean ± SD)	35.7 ± 10.2	34.6 ± 7.8	0.60
Use of intraluminal shunt	1 (11%)	2 (4%)	0.38

Figures 3 and **4** present chronological images of susceptibility differences obtained from QSM following ACZ administration, along with pre- and postoperative brain perfusion SPECT images from an individual with CH syndrome after surgery and an individual without postoperative CH, respectively.

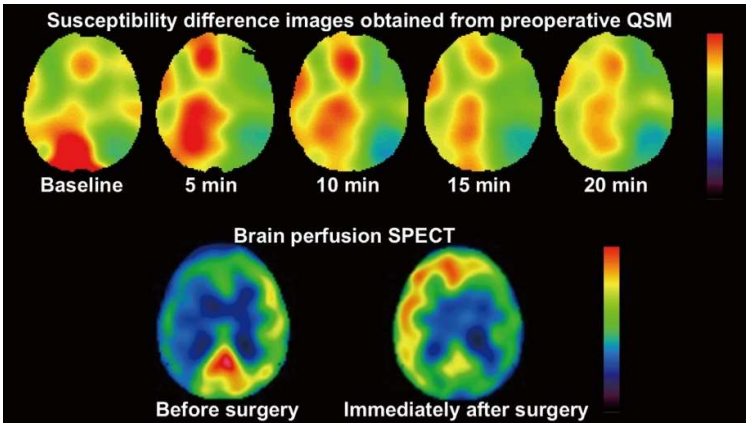

FIG 3. A 79-year-old woman with preoperative minor ischemic stroke resulting in left hemiparesis and bilateral cervical internal carotid artery stenosis who experienced cerebral hyperperfusion syndrome after carotid endarterectomy for right internal carotid artery stenosis. Susceptibility on susceptibility difference images (upper) obtained from preoperative quantitative susceptibility mapping (QSM) increases at 5 min after acetazolamide (ACZ) administration in the right cerebral hemisphere compared to baseline, suggesting early "steal" phenomenon. Susceptibility in that hemisphere begins to decline at 10 min after ACZ administration and falls below the baseline level at 20 min after ACZ administration. In contrast, susceptibility in the left cerebral hemisphere decreases at 5 min after ACZ administration compared to baseline, and this reduced susceptibility is maintained until 20 min after ACZ administration. Preoperative brain perfusion SPECT images show hypoperfusion in the right cerebral hemisphere (lower left), where hyperperfusion occurs immediately after surgery (lower right). At 5 days after surgery, left hemiparesis has deteriorated.

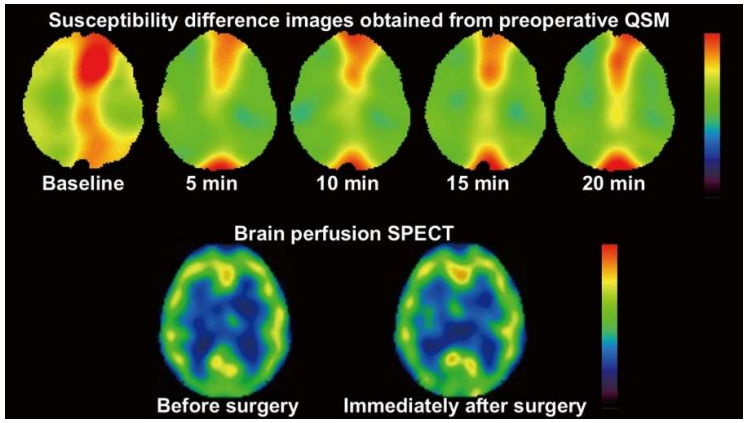

FIG 4. A 68-year-old man with preoperative minor ischemic stroke resulting in right hemiparesis who did not show cerebral hyperperfusion on brain perfusion SPECT after carotid endarterectomy for unilateral left internal carotid artery stenosis. Susceptibility on susceptibility difference images (upper) obtained from preoperative QSM is decreased in bilateral cerebral hemispheres at 5 min after ACZ administration compared to baseline. This reduced susceptibility is maintained until 20 min after ACZ administration. Pre- (lower left) and postoperative (lower right) brain perfusion SPECT images show no abnormal perfusion areas. The postoperative course was uneventful.

DISCUSSION (Online Supplemental Data)

We found that dynamic alterations in susceptibility after ACZ administration, which have been shown to reflect changes in OEF, using 7T MRI QSM before surgery predicted post-CEA CH with high accuracy. Based on the present and previous findings, those with access to 7T MRI should consider performing ACZ-loaded 7T MRI QSM in patients scheduled to undergo CEA. Any patient with an RSD_5 exceeding 102% should be deemed at high risk for CH following CEA and should undergo brain perfusion imaging immediately postoperatively. If CH is detected on this postoperative brain perfusion imaging, intensive blood pressure control should be initiated. The practical algorithm thereafter adheres to "*Pre-, intra-, and postoperative management*" as provided in the Online Supplemental Data.

A previous study showed that images of susceptibility differences between venous structures and surrounding brain tissue generated from QSM correlated with OEF images on PET and provided highly sensitive and specific detection of stage 2 ischemia or misery perfusion in the MCA territory.[26] Such static images generated from QSM without ACZ challenge can determine the post-CEA CH risk. However, whereas most patients who develop post-CEA CH have autoregulatory impairment, as shown in the present study, CH can also develop in patients without increased OEF, likely reflecting stage I hemodynamic impairment.[3] Static images of susceptibility differences may not identify this condition. Further, these images theoretically cannot detect variably increased CBV or distinguish conditions with increased OEF and increased CBV from those with increased OEF but normal CBV, yielding false-negative results and relatively low positive predictive values (45%) for predicting CH after CEA,[32] compared to values obtained in the present study using dynamic alterations in susceptibility differences after ACZ administration. In addition, a previous study employing static susceptibility-difference images without ACZ challenge used affected-to-contralateral asymmetry, making this method applicable only to patients with unilateral cervical ICA stenosis.[32] In contrast, the present study using dynamic alterations in susceptibility differences after ACZ administration included patients with bilateral ICA stenosis and allowed prediction of post-CEA CH even in these patients.

When cerebral metabolism is assumed to remain unchanged by ACZ, the dynamic changes in susceptibility observed in our patients with postoperative CH likely reflected increased OEF due to an early "steal" phenomenon of CBF, which occurs in territories experiencing autoregulatory failure (stage II hemodynamic impairment). CBV is reportedly increased in the territory experiencing an early "steal" phenomenon of CBF,[22,27] and previous research has indicated that preoperatively elevated CBV is associated with post-CEA CH.[18,19] However, while increased CBV as measured using perfusion-weighted or intravoxel incoherent motion MRI offered a 100% negative predictive value for predicting post-CEA CH, the positive predictive value for this prediction was poor (< 50%).[18,19] Both increased CBV and increased OEF are seen with more severe hemodynamic impairment,[17] and identifying increased OEF in areas with early "steal" of CBF likely leads to more accurate identification of stage II hemodynamic impairment with autoregulatory failure. This may explain why the dynamic alterations in susceptibility after ACZ administration used in the present study predicted post-CEA CH with high accuracy.

One previous study introduced images of susceptibility differences between small veins and surrounding tissue generated from QSM images obtained using 3T MRI and a method similar to that described in the present study and compared susceptibility differences with OEF on ^{15}O-gas PET.[33] When results from that study using QSM with 3T MRI were compared with those from a study using QSM with 7T MRI,[26] the susceptibility difference with 3T MRI exhibited only slight inferiority in terms of the correlation coefficient with OEF and the sensitivity/specificity for detecting increased OEF.[26] Considering those findings and the limited install base of 7T MR scanners, as well as limitations of scanning patients at 7T, the data obtained from the present study may be extrapolated to dynamic alterations in susceptibility after ACZ administration using 3T MRI QSM. Further investigations to determine whether this extrapolation is clinically useful for predicting post-CEA CH would be beneficial.

Blood oxygenation level-dependent cerebrovascular reactivity with CO_2 inhalation using a 3T MRI scanner reportedly harbors sufficient data to provide specific cerebrovascular reactivity cutoff points for hemodynamic failure staging across individual vascular territories.[34] However, unlike out study, that study included only patients with unilateral steno-occlusive disease and direct comparisons

were not performed with other hemodynamic factors such as CBV or cerebral oxygen metabolism.[34] Arterial spin-labeling imaging also allows evaluation of the distribution, magnitude, and time course of cerebrovascular response to ACZ.[35] However, the postlabeling delay-dependent difference was evident for regional CBF after ACZ injection and regional cerebrovascular reactivity, and obtaining the precise time course of cerebrovascular responses to ACZ thus may be difficult using this imaging in ICA steno-occlusive diseases.

Whereas the present study used single-echo gradient-recalled acquisition, multi-echo gradient-recalled acquisitions for QSM enable optimization of the SNR for several tissue types through multi-echo combinations or investigation of temporal variations in susceptibility (potentially reflecting tissue microstructure) by calculating one QSM image at each TE (TE-dependent QSM).[36] Technical limitations regarding the use of 7T MRI QSM in our study have been previously described.[26,27,32] Additionally, nearly 20% of patients did not undergo 7T MRI due to the presence of implantable electronic devices or metals, or because scanning was canceled due to side effects associated with ultra-high field MRI. Furthermore, in 5% of patients who underwent 7T MRI, sufficient data to generate QSM were not obtained due to motion artifacts. Motion artifacts are independent of both observable variables and unobservable parameters of interest, and occur entirely at random. Data with motion artifacts are thus missing completely at random and the present analyses performed using data excluding patients with motion artifacts may be considered unbiased. The Conover test used in the present study does not correct for the multiple comparisons problem. Statistical results of differences in RSD across time points might thus represent overestimates. As another limitation, although patients with exhausted cerebrovascular autoregulation in bilateral whole cerebral hemispheres due to bilateral steno-occlusive ICAs without communication with the posterior circulation (e.g., bilateral fetal-type ICAs with hypoplastic P1s in the posterior cerebral arteries bilaterally) would also have a high risk of CH following CEA, early “steal” phenomenon of CBF may not occur in such patients, resulting in false-negative predictions of CH following CEA.

CONCLUSIONS

We found that dynamic changes in susceptibility following ACZ administration, measured using 7T MRI QSM before surgery, accurately predict post-CEA CH development. Our work demonstrates the utility of ACZ-loaded QSM to inform peri-operative management of patients undergoing CEA to reduce the risk of CH. However, further work is needed to validate the findings at 3T which would allow this test to be performed in a larger number of patients and provide a more practical algorithm for reducing the risk of CH following CEA.

ACKNOWLEDGMENTS

None.

REFERENCES

1. Piepgras DG, Morgan MK, Sundt Jr TM, et al. Intracerebral hemorrhage after carotid endarterectomy. *J Neurosurg* 1988;68:532−536

2. Sundt Jr TM, Sharbrough FW, Piepgras DG, et al. Correlation of cerebral blood flow and electroencephalographic changes during carotid endarterectomy: with results of surgery and hemodynamics of cerebral ischemia. *Mayo Clin Proc* 1981;56:533−543

3. Oshida S, Ogasawara K, Saura H, et al. Does preoperative measurement of cerebral blood flow with acetazolamide challenge in addition to preoperative measurement of cerebral blood flow at the resting state increase the predictive accuracy of development of cerebral hyperperfusion after carotid endarterectomy? Results from 500 cases with brain perfusion single-photon emission computed tomography study. *Neurol Med Chir (Tokyo)* 2015;55:141−148

4. Bernstein M, Fleming JF, Deck JH. Cerebral hyperperfusion after carotid endarterectomy: a cause of cerebral hemorrhage. *Neurosurgery* 1984;15:50−56

5. Ogasawara K, Sakai N, Kuroiwa, et al. Intracranial hemorrhage associated with cerebral hyperperfusion syndrome following carotid endarterectomy and carotid artery stenting: retrospective review of 4494 patients. *J Neurosurg* 2007;107:1130−1136

6. van Mook WN, Rennenberg RJ, Schurink GW, et al. Cerebral hyperperfusion syndrome. *Lancet Neurol* 2005;4:877−888

7. Chida K, Ogasawara K, Suga Y, et al. Postoperative cortical neural loss associated with cerebral hyperperfusion and cognitive impairment after carotid endarterectomy: ^{123}I-iomazenil SPECT study. *Stroke* 2009;40:448−453

8. Nanba T, Ogasawara K, Nishimoto H, et al. Postoperative cerebral white matter damage associated with cerebral hyperperfusion and cognitive impairment after carotid endarterectomy: a diffusion tensor magnetic resonance imaging study. *Cerebrovasc Dis* 2012;34:358−367

9. Igarashi S, Ando T, Takahashi T, et al. Development of cerebral microbleeds in patients with cerebral hyperperfusion following carotid endarterectomy and its relation to postoperative cognitive decline. *J Neurosurg* 2021;135:1122−1128

10. Araya S, Akamatsu Y, Ono Y, et al. Impact of postoperative cerebral hyperperfusion on 2-year cognitive outcomes of patients undergoing carotid endarterectomy. *J Neurosurg* 2024 Aug 9. [Epub ahead of print]

11. Baron JC, Bousser MG, Rey A, et al. Reversal of focal "misery-perfusion syndrome" by extra-intracranial arterial bypass in hemodynamic cerebral ischemia: a case study with ^{15}O positron emission tomography. *Stroke* 1981;12:454−459

12. Gibbs JM, Wise RJ, Leenders KL, et al. Evaluation of cerebral perfusion reserve in patients with carotid-artery occlusion. *Lancet* 1984;1:310−314

13. Powers WJ, Raichle ME. Positron emission tomography and its application to the study of cerebrovascular disease in man. *Stroke* 1985;16:361−376

14. Yoshimoto T, Houkin K, Kuroda S, et al. Low cerebral blood flow and perfusion reserve induce hyperperfusion after surgical revascularization: case reports and analysis of cerebral hemodynamics. *Surg Neurol* 1997;48:132−138

15. Hosoda K, Kawaguchi T, Shibata Y, et al. Cerebral vasoreactivity and internal carotid artery flow help to identify patients at risk for hyperperfusion after carotid endarterectomy. *Stroke* 2001;32:1567−1573

16. Ogasawara K, Yukawa H, Kobayashi M, et al. Prediction and monitoring of cerebral hyperperfusion after carotid endarterectomy by using single-photon emission computerized tomography scanning. *J Neurosurg* 2003;99:504−510

17. Derdeyn CP, Videen TO, Yundt KD, et al. Variability of cerebral blood volume and oxygen extraction: stages of cerebral haemodynamic impairment revisited. *Brain* 2002;125: 595−607

18. Fukuda T, Ogasawara K, Kobayashi M, et al. Prediction of cerebral hyperperfusion after carotid endarterectomy using cerebral blood volume measured by perfusion-weighted MR imaging compared with single-photon emission CT. *AJNR Am J Neuroradiol* 2007;28:737−742

19. Takahashi T, Uwano I, Akamatsu Y, et al. Prediction of cerebral hyperperfusion following carotid endarterectomy using intravoxel incoherent motion magnetic resonance imaging. *J Stroke Cerebrovasc Dis* 2023;32:106909

20. Reinhard M, Muller T, Roth M, et al. Bilateral severe carotid artery stenosis or occlusion: cerebral autoregulation dynamics and collateral flow patterns. *Acta Neurochir (Wien)* 2003;145:1053−1060

21. Edwin M. Nemoto EM, Yonas H, Chang Y. Stages and thresholds of hemodynamic failure. *Brain* 2003;34:2−3

22. Kobayashi M, Igarashi S, Takahashi T, et al. Optimal timing for measuring cerebral blood flow after acetazolamide administration to detect preexisting cerebral hemodynamics and metabolism in patients with bilateral major cerebral artery steno-occlusive diseases: ^{15}O positron emission tomography studies. *Am J Nucl Med Mol Imaging* 2021; 11:507−518

23. Zhang J, Liu T, Gupta A, et al. Quantitative mapping of cerebral metabolic rate of oxygen (CMRO2) using quantitative susceptibility mapping (QSM). *Magn Reson Med* 2015;74:945–952

24. De Vis JB, Petersen ET, Bhogal A, et al. Calibrated MRI to evaluate cerebral hemodynamics in patients with an internal carotid artery occlusion. *J Cereb Blood Flow Metab* 2015;35:1015–1023

25. Liu Z, Li Y. Cortical cerebral blood flow, oxygen extraction fraction, and metabolic rate in patients with middle cerebral artery stenosis or acute stroke. *AJNR Am J Neuroradiol* 2016;37:607–614

26. Uwano I, Kudo K, Sato R, et al. Noninvasive assessment of oxygen extraction fraction in chronic ischemia using quantitative susceptibility mapping at 7 Tesla. *Stroke* 2017;48:2136–2141

27. Fujimoto K, Uwano I, Sasaki M, et al. Acetazolamide-loaded dynamic 7T MR quantitative susceptibility mapping in major cerebral artery steno-occlusive disease: comparison with PET. *AJNR Am J Neuroradiol* 2020;41:785–791

28. North American Symptomatic Carotid Endarterectomy Trial Collaborators. Beneficial effect of carotid endarterectomy in symptomatic patients with high-grade carotid stenosis. *N Engl J Med* 1991;325:445–453

29. Ashburner J. SPM: a history. *Neuroimage* 2012;62:791-800

30. Takeuchi R, MatsudaH, YoshiokaK, et al. Cerebral blood flow SPET in transient global amnesia with automated ROI analysis by 3DSRT. *Eur J Nucl Med Mol Imaging* 2004;31:578–589

31. Yushkevich PA, Piven J, Hazlett HC, et al. User-guided 3D active contour segmentation of anatomical structures: significantly improved efficiency and reliability. *Neuroimage* 2006;31:1116–1128

32. Nomura JI, Uwano I, Sasaki M, et al. Preoperative cerebral oxygen extraction fraction imaging generated from 7T MR quantitative susceptibility mapping predicts development of cerebral hyperperfusion following carotid endarterectomy. *AJNR Am J Neuroradiol* 2017;38:2327–2333

33. Kudo K, Liu T, Murakami T, et al. Oxygen extraction fraction measurement using quantitative susceptibility mapping: comparison with positron emission tomography. *J Cereb Blood Flow Metab* 2016;36:1424–1433

34. Sebök M, van der Wouden F, Mader C, et al. Hemodynamic failure staging with blood oxygenation level-dependent cerebrovascular reactivity and acetazolamide-challenged (^{15}O-) H_2O-positron emission tomography across individual cerebrovascular territories. *J Am Heart Assoc* 2023;12:e029491

35. Inoue Y, Tanaka Y, Hata H, et al. Arterial spin-labeling evaluation of cerebrovascular reactivity to acetazolamide in healthy subjects. *AJNR Am J Neuroradiol* 2014;35:1111–1116

36. Biondetti E, Karsa A, Thomas DL, et al. Investigating the accuracy and precision of TE-dependent versus multi-echo QSM using Laplacian-based methods at 3 T. *Magn Reson Med* 2020;84:3040–3053

SUPPLEMENTAL FILES

On-line Figure 1

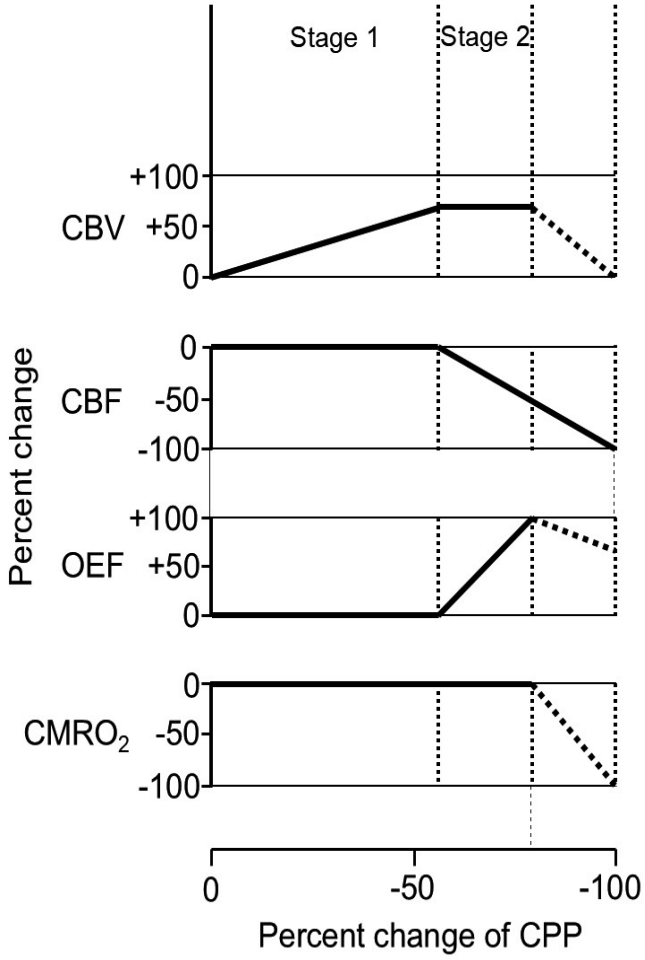

Illustration of changes in each cerebral perfusion or metabolic variable with progressive decreases in cerebral perfusion pressure (CPP). This is a modification of an illustration by Powers et al.[1] CBV, cerebral blood volume; CBF, cerebral blood flow; OEF, oxygen extraction fraction; $CMRO_2$, cerebral metabolic rate for oxygen. In stage I ischemia, CBV begins to increase, but CBF, OEF and $CMRO_2$ are unchanged. In stage II ischemia, CBV is maximally increased and CBF begins to decrease. However, OEF begins to increase, resulting in preservation of $CMRO_2$. Dashed lines after stage 2 ischemia show postulated changes.

1. Powers WJ, Raichle ME. Positron emission tomography and its application to the study of cerebrovascular disease in man. *Stroke* 1985;16:361−376

On-line MRI protocol and generation of QSM

QSM images were generated from source images using an in-house program with multiple dipole-inversion combination with *k*-space segmentation[1] and regularization-enabled sophisticated harmonic artifact reduction for phase data methods.[2] A two-dimensional Gaussian low-pass filter with a kernel size of 60% of the total image power in each section was applied to extract iron deposition in deep nuclei, hemosiderin deposition, dural sinuses, and large venous structures, and a two-dimensional Gaussian high-pass filter of 2% was applied to extract small venous structures.[3] Small venous structures were then determined by multiplying the Gaussian high-pass filter-processed binary images and the logical negations of Gaussian low-pass filter-processed binary images under the threshold for binarization of > +2 standard deviations.[3]

Images of susceptibility differences between the average susceptibility of small veins and surrounding tissue were generated from the above-mentioned QSM images using a method similar to that described in the previous study.[4] First, a venous mask was created using a local threshold method with a voxel-of-interest of 25 mm^3. A local threshold value of mean +2 standard deviations was used for the segmentation of venous voxels in the voxel-of-interest, based on the idea that susceptibility of the vein becomes higher than that of brain parenchyma due to elevated levels of deoxy-hemoglobin. After segmentation of venous pixels, the susceptibility difference between the average susceptibility of veins and surrounding tissue was calculated in each voxel-of-interest. The susceptibility difference was finally displayed with a smoothing procedure.

1. Sato R, Shirai T, Taniguchi Y, et al. Quantitative susceptibility mapping using the multiple dipole-inversion combination with *k*-space segmentation method. *Magn Reson Med Sci* 2017;16:340–50

2. Sun H, Wilman AH. Background field removal using spherical mean value filtering and Tikhonov regularization. *Magn Reson Med*

2014;71:1151–1157

3. Uwano I, Kudo K, Sato R, et al. Noninvasive assessment of oxygen extraction fraction in chronic ischemia using quantitative susceptibility mapping at 7 Tesla. *Stroke* 2017;48:2136–2141

4. Kudo K, Liu T, Murakami T, et al. Oxygen extraction fraction measurement using quantitative susceptibility mapping: comparison with positron emission tomography. *J Cereb Blood Flow Metab* 2016;36:1424–1433

On-line Brain perfusion SPECT

Quantitative brain perfusion SPECT with iodine-123 N-isopropyl-p-iodoamphetamine (^{123}I-IMP) was performed within 7 days before and immediately after CEA to detect CH, as previously described.[1] On the third day post-CEA, patients who exhibited CH underwent a third ^{123}I-IMP SPECT following the same protocol. Quantitative CBF images were generated using the ^{123}I-IMP autoradiography method.[1]

1. Ogasawara K, Ito H, Sasoh M, et al. Quantitative measurement of regional cerebrovascular reactivity to acetazolamide using ^{123}I-N-isopropyl-p-iodoamphetamine autoradiography with SPECT: validation study using $H_2{}^{15}O$ with PET. *J Nucl Med* 2003;44:520–525

On-line Figure 2

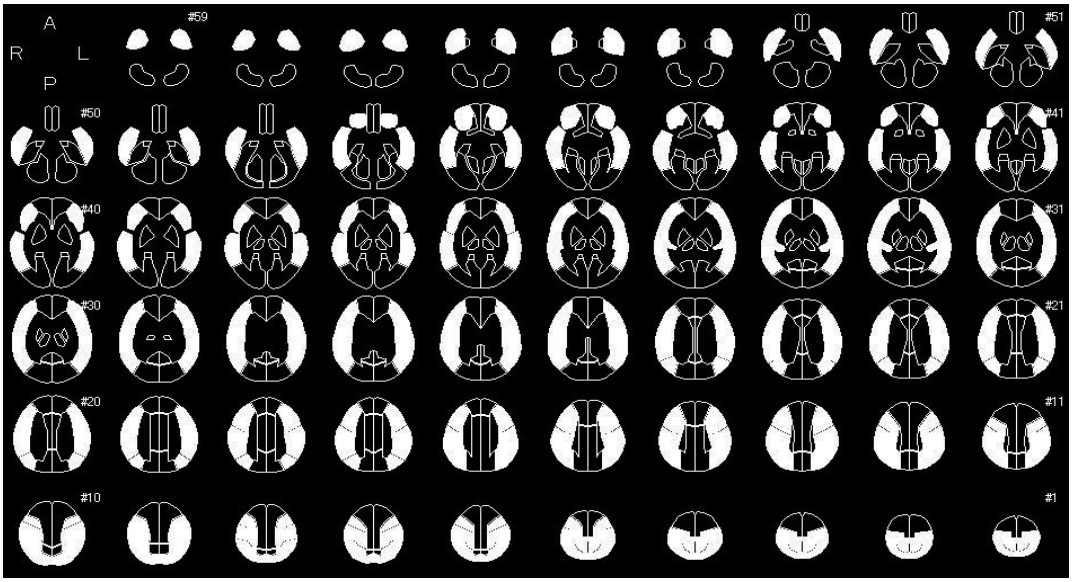

Diagrams showing the five ROIs indicating territories perfused by bilateral MCAs (white) for the 3D stereotaxic ROI template.

On-line Pre-, Intra-, And Postoperative Management

Antiplatelets were administered until the morning of the CEA, which was performed under general anesthesia.[1] A bolus of 5000 IU of heparin was administered prior to ICA clamping.[1] An intraluminal shunt was placed based on the findings of intraoperative electroencephalography using a 12-channel montage.[2,3] Postoperatively, intravenous antihypertensive medications were used to maintain arterial blood pressure between 100 and 140 mmHg in patients identified with post-CEA CH on brain perfusion SPECT.[1] Blood pressure management was discontinued in patients with resolved CH, as indicated by brain perfusion SPECT conducted on the third postoperative day.[1] In patients exhibiting CH syndrome,[1] a propofol coma was induced, which was detected based on the following criteria: (1) new or worsening seizures, alterations in the level of consciousness, and/or focal neurological signs (e.g., motor weakness) occurring 24 hours to 30 days postoperatively; and (2) evidence of CH on brain perfusion SPECT.[1]

1. Oshida S, Ogasawara K, Saura H, et al. Does preoperative measurement of cerebral blood flow with acetazolamide challenge in addition to preoperative measurement of cerebral blood flow at the resting state increase the predictive accuracy of development of cerebral hyperperfusion after carotid endarterectomy? Results from 500 cases with brain perfusion single-photon emission computed tomography study. *Neurol Med Chir (Tokyo)* 2015;55:141−148

2. Igarashi S, Ando T, Takahashi T, et al. Development of cerebral microbleeds in patients with cerebral hyperperfusion following carotid endarterectomy and its relation to postoperative cognitive decline. *J Neurosurg* 2021;135:1122−1128

3. Araya S, Akamatsu Y, Ono Y, et al. Impact of postoperative cerebral hyperperfusion on 2-year cognitive outcomes of patients undergoing carotid endarterectomy. *J Neurosurg* 2024 Aug 9. [Epub ahead of print]

On-line Statistical Analysis

The sample size was determined based on prior studies.[1,2] Postoperative CH on brain perfusion SPECT was estimated to develop in

45% of individuals with increased CBV and 5% of those without increased CBV. The ratio of patients with increased CBV to those without was estimated to be 0.25. Consequently, a total of 58 patients was required to achieve a statistical power of 80% and an α error of 5% to detect a 40% difference in the development of postoperative CH on brain perfusion SPECT using Fisher's exact test. Anticipating that some patients may generate insufficient QSM data due to motion artifacts, we aimed to enroll 65 patients.

Data are expressed as mean ± standard deviation (SD). The Shapiro–Wilk test was used to determine whether relative susceptibility difference (RSD) data obtained at each time point in patients with or without postoperative CH showed normal distributions. When data were normally distributed, differences in RSD across time points were evaluated using one-way repeated-measures analysis of variance (ANOVA), followed by the Scheffe test as a post-hoc analysis. When data were not normally distributed, differences were evaluated using the Friedman test, followed by the Conover test as a post-hoc analysis. Receiver operating characteristic (ROC) curves were employed to compare the accuracy of predicting the development of postoperative CH based on RSD at each time point after ACZ administration. Pairwise comparisons of the area under the ROC curve for RSD at each time point were performed, using the method proposed by DeLong et al.[3] The cutoff lying closest to the upper left corner of the ROC curve for predicting the development of postoperative CH was determined for RSD at each time point. The 95% CIs for sensitivity, specificity, and positive and negative predictive values were calculated using binomial distributions. Univariate analysis, employing the Mann–Whitney U test or Fisher's exact test, was performed to explore the relationship between postoperative CH and each variable, including the RSD with the highest area under the ROC curve. Logistic regression analysis of variables associated with CH was performed using a sequential backward elimination approach. Exclusion of explanatory variables was halted when the p-value of the remaining variables reached < 0.2. Before logistic regression analysis was performed, we had tested relationships among any two explanatory variables using the Mann–Whitney U test, Fisher's exact test or Spearman's rank correlation coefficient to check for multicollinearity. Logistic regression analysis using a sequential backward elimination approach was performed with the following two models: inclusion (with multicollinearity) and exclusion (without multicollinearity) of explanatory variables with significant relationships. However, only RSD_5 remained as an explanatory variable in the model with exclusion. P-values < 0.05 were considered significant.

1. Fukuda T, Ogasawara K, Kobayashi M, et al. Prediction of cerebral hyperperfusion after carotid endarterectomy using cerebral blood volume measured by perfusion-weighted MR imaging compared with single-photon emission CT. *AJNR Am J Neuroradiol* 2007;28:737−742

2. Takahashi T, Uwano I, Akamatsu Y, et al. Prediction of cerebral hyperperfusion following carotid endarterectomy using intravoxel incoherent motion magnetic resonance imaging. *J Stroke Cerebrovasc Dis* 2023;32:106909

3. DeLong ER, DeLong DM, Clarke-Pearson DL. Comparing the areas under two or more correlated receiver operating characteristic curves: a nonparametric approach. *Biometrics* 1988;44:837–845

On-line Result 1

RSD_5 was significantly higher in patients with bilateral steno-occlusive lesions than in those without such lesions ($p < 0.05$). RSD_5 also correlated significantly with the degree of ICA stenosis ($\rho = 0.35$, $p < 0.05$). No significant relationships were observed among the other two explanatory variables.

First, we analyzed our data using logistic regression analysis with a sequential backward elimination approach **including** bilateral steno-occlusive lesions and degree of ICA stenosis. When RSD_5, bilateral steno-occlusive lesions and degree of ICA stenosis remained as explanatory variables, the p values for bilateral steno-occlusive lesions and degree of ICA stenosis were >0.2 and these two explanatory variables were further excluded from logistic regression analysis. Eventually, only RSD_5 remained as an explanatory variable (95%CI, 455.9–4043.6; p = 0.0281).

Next, we analyzed our data using logistic regression analysis with a sequential backward elimination approach **excluding** bilateral steno-occlusive lesions and degree of ICA stenosis. Eventually, only RSD_5 remained as an explanatory variable (95%CI, 455.9–4043.6; p = 0.0281).

Logistic regression analysis in both models with and without multicollinearity thus revealed the same result.

On-line Result 2

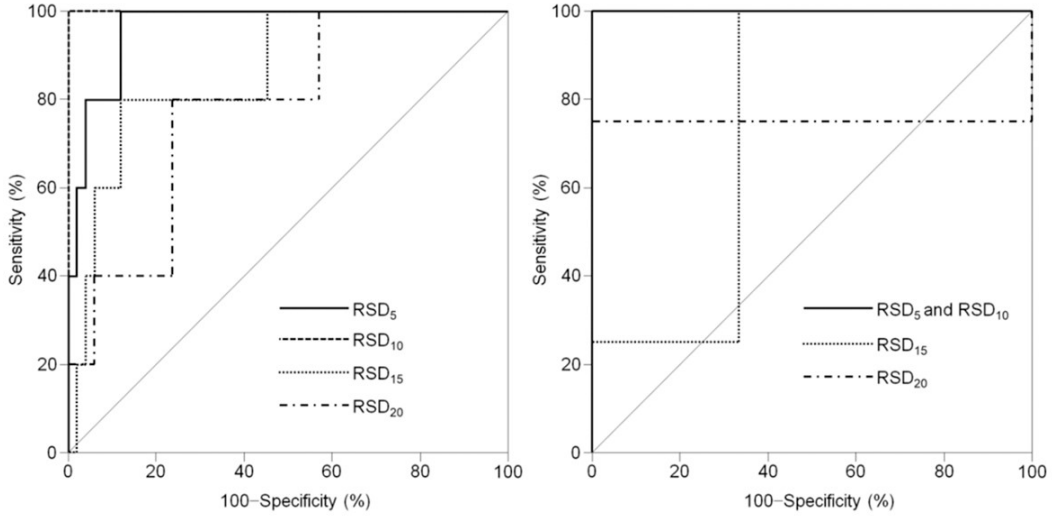

Illustrations of the comparison of ROC curves for predicting CH immediately after surgery based on RSD at various time points following ACZ administration. A total of 63 patients included in the present study were stratified to 56 with a unilateral steno-occlusive lesion (left graph) and 7 with bilateral steno-occlusive lesions (right graph).

For 56 patients with a unilateral steno-occlusive lesion, the area under the ROC curve was significantly greater for RSD_{10} (1.000; 95% CI, 0.936–1.000) compared to RSD_{20} (0.780; 95% CI, 0.650–0.880) ($p < 0.05$). No significant differences among other combinations including RSD_5 (0.965; 95% CI, 0.877–0.996) and RSD_{15} (0.863; 95% CI, 0.744–0.940) were observed.

For 7 patients with bilateral steno-occlusive lesions, areas under the ROC curve were as follows: 1.000 (95% CI, 0.590–1.000) for RSD_5, 1.000 (95% CI, 0.590–1.000) for RSD_{10}, 0.750 (95% CI, 0.321–0.975) for RSD_{15}, and 0.750 (95% CI, 0.321–0.975) for RSD_{20}. No differences among any combinations of RSD at each time point after ACZ administration were observed.

For 56 patients with a unilateral steno-occlusive lesion, sensitivity, specificity, and positive and negative predictive values for RSD at each time point after ACZ administration, calculated at the cutoff closest to the upper left corner of the ROC curve for predicting CH, are presented in the following table.

	RSD_5	RSD_{10}	RSD_{15}	RSD_{20}
Sensitivity	100%	100%	80%	80%
95% CI	100–100%	100–100%	28–99%	28–99%
Specificity	88%	100%	88%	76%
95% CI	76–96%	100–100%	76–96%	63–87%
Positive-predictive value	46%	100%	40%	25%
95% CI	28–64%	100–100%	22–61%	15–39%
Negative-predictive value	100%	100%	98%	98%
95% CI	100–100%	100–100%	89–99%	87–99%
Cutoff value (%)	102	103	98	96

Among these four metrics, RSD_{10} basically exhibited the highest values, followed by RSD_5, RSD_{15}, and RSD_{20}.

For 7 patients with bilateral steno-occlusive lesions, sensitivity, specificity, and positive and negative predictive values for RSD at each time point after ACZ administration, calculated at a cutoff closest to the upper left corner of the ROC curve for predicting CH, are presented in the following table.

	RSD_5	RSD_{10}	RSD_{15}	RSD_{20}
Sensitivity	100%	100%	100%	75%
95% CI	100–100%	100–100%	100–100%	19–99%
Specificity	100%	100%	67%	100%
95% CI	100–100%	100–100%	9–99%	100–100%
Positive-predictive value	100%	100%	80%	100%
95% CI				

	100–100%	100–100%	15–95%	100–100%
Negative-predictive value 95% CI	100% 100–100%	100% 100–100%	100% 100–100%	75% 36–94%
Cutoff value (%)	97	95	91	95

Among these four metrics, RSD_5 and RSD_{10} basically exhibited the highest values, followed by RSD_{15} or RSD_{20}.

On-line Discussion

The chronological decreases in the accuracy of susceptibility changes after ACZ administration in predicting postoperative CH may also correspond to the later resolution of the "steal" phenomenon. Interestingly, the accuracy of predicting postoperative CH did not significantly differ between susceptibility changes at 5 and 10 min after ACZ administration. The examination times for these two intervals were approximately 11 and 18 min, respectively. Therefore, measuring susceptibility changes within the first 5 min after ACZ administration should be sufficient for predicting postoperative CH.

Measurement of cerebrovascular reactivity using brain perfusion SPECT with an ACZ challenge is the most common strategy for preoperative prediction of CH following carotid interventions.[1] In this approach, the tracer for SPECT is injected intravenously 10 min after ACZ administration, with data acquisition performed at a mid-scan time of 30 min post-injection for a scan duration of 20 min.[2] According to a study investigating chronological changes in CBF after ACZ administration using ^{15}O-gas PET,[3] such a SPECT protocol detects an average of late stable conditions rather than early dynamic changes in CBF. This difference in study protocols between conventional brain perfusion SPECT and the present 7T MRI QSM may explain the relatively higher positive predictive value of the latter (60%) for predicting CH following CEA, compared to the former's value of 45%,[4] although the present study did not directly compare data obtained using the two modalities.

Our results showed that the incidence of bilateral steno-occlusive lesions, the degree of ICA stenosis ipsilateral to surgery, and susceptibility changes at 5 min after ACZ administration were significantly greater in patients with CH immediately postoperatively than in those without CH. However, the first two factors were not significant predictors of CH in logistic regression analysis. These two factors are considered classical risk factors for CH following CEA, as they often contribute to compromised cerebral hemodynamics.[5,6]

1. Ogasawara K. Single photon emission computed tomography (SPECT). In: Gillard J, Graves M, Hatsukami T, Kuan C, eds. *Carotid diseases: the role of imaging in diagnosis and management* 1st ed. Cambridge: Cambridge University Press; 2007:387–395

2. Ogasawara K, Ito H, Sasoh M, et al. Quantitative measurement of regional cerebrovascular reactivity to acetazolamide using ^{123}I-N-isopropyl-p-iodoamphetamine autoradiography with SPECT: validation study using $H_2{}^{15}O$ with PET. *J Nucl Med* 2003;44:520–525

3. Kobayashi M, Igarashi S, Takahashi T, et al. Optimal timing for measuring cerebral blood flow after acetazolamide administration to detect preexisting cerebral hemodynamics and metabolism in patients with bilateral major cerebral artery steno-occlusive diseases: ^{15}O positron emission tomography studies. *Am J Nucl Med Mol Imaging* 2021; 11:507−518

4. Oshida S, Ogasawara K, Saura H, et al. Does preoperative measurement of cerebral blood flow with acetazolamide challenge in addition to preoperative measurement of cerebral blood flow at the resting state increase the predictive accuracy of development of cerebral hyperperfusion after carotid endarterectomy? Results from 500 cases with brain perfusion single-photon emission computed tomography study. *Neurol Med Chir (Tokyo)* 2015;55:141−148

5. Reigel MM, Hollier LH, Sundt TM, et al. Cerebral hyperperfusion syndrome: a cause of neurologic dysfunction after carotid endarterectomy. *J Vasc Surg* 1987;5:628–634

6. Hosoda K, Kawaguchi T, Shibata Y, et al. Cerebral vasoreactivity and internal carotid artery flow help to identify patients at risk for hyperperfusion after carotid endarterectomy. *Stroke* 2001;32:1567–1573